



Boundary layer versus free tropospheric submicron particle formation: A case study from NASA DC-8 observations in the Asian continental outflow during the KORUS-AQ campaign

Do-Hyeon Park^a, Chaeyoon Cho^a, Hyeonmin Kim^a, Rokjin J. Park^a, Bruce Anderson^b, Taehyoung Lee^c, Greg L. Huey^d, Paul O. Wennberg^e, Andrew J. Weinheimer^f, Seong Soo Yum^g, Russell Long^h, Sang-Woo Kim^{a,*}

^a School of Earth and Environmental Sciences, Seoul National University, Seoul, Republic of Korea

^b NASA Langley Research Center, Hampton, VA, USA

^c Department of Environmental Science, Hankuk University of Foreign Studies, Republic of Korea

^d School of Earth and Atmospheric Sciences, Georgia Institute of Technology, Atlanta, GA, USA

^e California Institute of Technology, Pasadena, CA, USA

^f National Center for Atmospheric Research, Boulder, CO, USA

^g Department of Atmosphere Science, Yonsei University, Seoul, Republic of Korea

^h Office of Research and Development, U.S. EPA, Research Triangle Park, NC, USA

ARTICLE INFO

Keywords:

Submicron particle formation
Secondary inorganic aerosols
Boundary layer
Free troposphere
KORUS-AQ

ABSTRACT

In this study, we contrasted major secondary inorganic species and processes responsible for submicron particle formation (SPF) events in the boundary layer (BL) and free troposphere (FT) over the Korean Peninsula during Korea-United States Air Quality (KORUS-AQ) campaign (May–June 2016) using aircraft observations. The number concentration of ultrafine particles with diameters between 3 nm and 10 nm ($N_{\text{CN3-10}}$) during the entire KORUS-AQ period reached a peak ($7606 \pm 12,003 \text{ cm}^{-3}$) at below 1 km altitude, implying that the particle formation around the Korean Peninsula primarily occurred in the daytime BL. During the BL SPF case (7 May 2016), the SPF over Seoul metropolitan area was more attributable to oxidation of NO_2 rather than SO_2 -to-sulfate conversion. From the analysis of the relationship between nitrogen oxidation ratio (NOR) and temperature or relative humidity (RH), NOR showed a positive correlation only with temperature. This suggests that homogeneous gas-phase reactions of NO_2 with OH or O_3 contributed to nitrate formation. From the relationship between $N_{\text{CN3-10}}$ ($> 10,000 \text{ cm}^{-3}$) and the NOR (or sulfur oxidation ratio) at Olympic Park in Seoul during the entire KORUS-AQ period, it was regarded that the relative importance of nitrogen oxidation was grown as the $N_{\text{CN3-10}}$ increased. During the FT SPF case (31 May 2016) over the yellow sea, the SO_2 -to-sulfate conversion seemed to influence SPF highly. The sulfate/CO ratio had a positive correlation with both the temperature and RH, suggesting that aqueous-phase pathways as well as gas-phase reactions might be attributable to sulfate formation in the FT. In particular, FT SPF event on 31 May was possibly caused by the direct transport of SO_2 precursors from the continent above the shallow marine boundary layer under favorable conditions for FT SPF events, such as decreased aerosol surface area and increased solar radiation.

1. Introduction

Many regions in East Asia, like China or the Korean Peninsula, have suffered from extreme haze events brought on by elevated concentrations of $\text{PM}_{2.5}$ (particulate matter with diameters $\leq 2.5 \mu\text{m}$) (Liu et al., 2019; Park et al., 2021). Particularly, secondary inorganic species such

as sulfate, nitrate, and ammonium made up a substantial part (about 47%) of $\text{PM}_{2.5}$ in Seoul during the Korea-United States Air Quality (KORUS-AQ) campaign (May–June 2016), suggesting that the formation of submicron particles can play a significant role in the occurrence of haze events (Wang et al., 2016; NIER and NASA, 2017; Chu et al., 2020). Because such frequently occurring haze events are widely known to

* Corresponding author.

E-mail address: sangwookim@snu.ac.kr (S.-W. Kim).

<https://doi.org/10.1016/j.atmosres.2021.105857>

Received 13 May 2021; Received in revised form 14 September 2021; Accepted 14 September 2021

Available online 16 September 2021

0169-8095/© 2021 Published by Elsevier B.V.

create adverse effects on human health (Hanafi et al., 2019; Jiang et al., 2020; Zeng et al., 2020), it is crucial to determine the characteristics of submicron particle formation (SPF) that are associated with the dominant precursors or possible physical and chemical mechanisms to establish efficient mitigation strategies for secondary inorganic species.

Numerous types of observational evidence have indicated that submicron particles can be produced in the boundary layer (BL) by various precursor gases through complex chemical mechanisms. The formation of sulfate is largely fulfilled in the aqueous surface of aerosol particles or cloud droplets (He et al., 2014; Hung and Hoffmann, 2015; Cheng et al., 2016; Liu et al., 2020b), although the formation of sulfuric acid via gas-phase reactions of sulfur dioxide (SO₂) with hydrogen oxide (OH) can also be important for generating sulfate (Sander and Seinfeld, 1976; Ji et al., 2018). Recently, several studies have analyzed new particle formation (NPF) events driven by sulfuric acid (H₂SO₄) precursors at a molecular level. Yao et al. (2018) observed initial clusters of NPF and suggested that H₂SO₄-dimethylamine (DMA)-water (H₂O) nucleation has a crucial role in NPF in megacities of China. Myllys et al. (2019) introduced a molecular-level explanation for nanoparticle production through H₂SO₄-DMA-ammonia (NH₃) cluster formation. For nitrate, dinitrogen pentoxide (N₂O₅) can act as a reservoir of NO_x during the nighttime, and nitric acid (HNO₃) is subsequently formed by heterogeneous hydrolysis of N₂O₅, which is thermally decomposed and photolyzed during the day (Russell et al., 1986; Liu et al., 2020a). While the nighttime chemistry of nitrate episodes can be relatively well understood, the dominant pathways during the daytime are controversial (Tao et al., 2018; Tian et al., 2019). In addition to the typical gas-phase oxidation of nitrogen dioxide (NO₂) with OH or O₃ (Richards, 1983; Khoder, 2002; Alexander et al., 2009; Liu et al., 2020b), more complicated reactions such as nitrate formation in cloud water have been proposed (Tao et al., 2018).

Given the favorable conditions for SPF (e.g., reduced surface area or increased solar insolation), the free troposphere (FT) can be a significant origin of the newly formed particles (Song et al., 2010; Rose et al., 2017; Qi et al., 2019; Takegawa et al., 2020). Furthermore, particles formed in the FT can be entrained to the BL, thereby influencing on the air quality of the BL (Kerminen et al., 2018; Takegawa et al., 2020). However, despite the importance of SPF in the FT, few observations in the FT actually exist since they can only be conducted through limited methods, such as mountain-top observations (Bianchi et al., 2016; Shen et al., 2018; Lv et al., 2018). Although SPF events captured by ground-based observation in the mountain-top site can be related to the FT (Rose et al., 2017), they are also often associated with the air mass originated from the BL following the daytime valley wind (Rodríguez et al., 2009; Shen et al., 2016). The characteristics of FT SPF can be similar to the that of BL SPF under the daytime valley breeze, but relatively small amount of condensable vapors can result in the active FT SPF under above-mentioned favorable conditions compared to BL (Takegawa et al., 2020).

Various optical, physical, and chemical properties of aerosols related to SPF in the FT as well as BL were observed through the synergetic use of continuous ground-based observations and twenty research flights over the Korean Peninsula during the KORUS-AQ campaign. Based on the airborne and ground-level observations, we contrasted the major secondary inorganic species and possible processes responsible for SPF events in the BL and FT during the KORUS-AQ campaign. An overview of SPF characteristics based on the vertical profile of the number size distribution during the KORUS-AQ campaign is provided in the Section 3. An analysis of the possible causes during the BL and FT SPF cases of the KORUS-AQ and a characterization that extends to the entire period of KORUS-AQ over the Korean Peninsula are given in Section 4.

2. Measurements and data

In this study, we used measurements collected onboard twenty research flights of the NASA DC-8 aircraft and at a ground station

located in Seoul during the KORUS-AQ field campaign. The measured parameters and uncertainties of the instruments are given in Table 1.

For the airborne observations, the number concentrations of aerosols with diameters greater than 3 nm and 10 nm were observed by the condensation particle counter (CPC)-3776 and CPC-3010, respectively, by projecting light onto the aerosols and detecting the scattered-light pulses (Park et al., 2020). The size distributions of 10–199.5 nm mobility diameter aerosols were obtained from a scanning mobility particle sizer (SMPS) by counting the number of aerosols segregated in the differential mobility size analyzer (DMA) column according to their electrical mobility (Jeong and Evans, 2009; Kim et al., 2013, 2016). Sulfate and nitrate concentrations with diameters less than 1 μm were measured by an aerosol mass spectrometer (AMS) that classified ionized species according to their nominal mass and quantified the concentration of non-refractory particulate masses of chemically speciated submicron aerosols (DeCarlo et al., 2006). For the gas species, Caltech and Georgia-Tech chemical ionization mass spectrometer (CIMS) were used to measure the HNO₃ and SO₂ mixing ratios, respectively (Huey et al., 2004; Slusher et al., 2004; Crounse et al., 2006). Also, the NO₂ mixing

Table 1

Descriptions for the instruments and measured parameters in this study.

Platform	Instrument	Parameter	Uncertainty	Reference
Airborne	Condensation Particle Counter (CPC)	Aerosol number concentration with diameters greater than 3 nm and 10 nm [cm ⁻³]	10%	Park et al. (2020)
	Scanning mobility particle sizer (SMPS)	Particle size distribution [cm ⁻³]	20%	Jeong and Evans (2009) Kim et al. (2013) Kim et al. (2016)
	Aerosol mass spectrometer (AMS)	Sulfate and nitrate concentration (diameter < 1 μm) [μg m ⁻³]	Variable	DeCarlo et al. (2006)
	Chemical ionization mass spectrometer (CIMS)	Sulfur dioxide (SO ₂) and Nitric acid (HNO ₃) mixing ratio [pptv]	(30%) for SO ₂ (30% + 50 pptv) for HNO ₃	Huey et al. (2004) Slusher et al. (2004) Crounse et al. (2006)
	4-channel chemiluminescence instrument	Nitrogen dioxide (NO ₂) mixing ratio [pptv]	30% + 50 pptv	Weinheimer et al. (1993)
	Condensation particle counter (CPC)	Aerosol number concentration with diameters greater than 3 nm and 10 nm [cm ⁻³]	10%	Kim et al. (2020b) Kim et al. (2020c)
Ground	MARGA ADI2080	Sulfate and nitrate Concentration (diameter < 2.5 μm) [μg m ⁻³]	5%	Choi et al. (2019)
	SO ₂ analyzer (MEZUS-110)	Sulfur dioxide (SO ₂) mixing ratio [ppbv]	1%	Kim et al. (2020a)
	Teledyne T500U CAPS analyzer	Nitrogen dioxide (NO ₂) mixing ratio [ppbv]	10%	Nowlan et al. (2016)

ratio was obtained from the NCAR 4-channel NO_{xy}O_3 chemiluminescence instrument, which induces a chemiluminescent reaction by adding reagent O_3 to the sample flow (Weinheimer et al., 1993).

Ground observations were conducted at Olympic Park (37.52°N, 127.12°E; 26 m above mean sea level) in Seoul. The number concentrations of aerosols with diameters greater than 3 nm and 10 nm were derived from the same instruments (CPC-3776 and CPC-3010) used for the airborne measurements (Kim et al., 2020b, 2020c). The concentrations of inorganic species such as sulfate and nitrate in $\text{PM}_{2.5}$ were measured by the Monitor for Aerosols & Gases in Ambient Air (MARGA ADI2080), which takes advantage of ion chromatography to separate ions according to their charges (Choi et al., 2019). The SO_2 mixing ratio was obtained from the KENTEK SO_2 analyzer (MEZUS-110) by applying an ultraviolet fluorescent method (Kim et al., 2020a). Lastly, the NO_2 mixing ratio was estimated by the Teledyne T500U CAPS analyzer using a cavity attenuated phase shift (CAPS) technique (Nowlan et al., 2016). More details related to the instrumentation mentioned above can be found in the literature listed in Table 1.

We also used the three-dimensional global chemical transport model, GEOS-Chem (Bey et al., 2001; Oak et al., 2019), for the East Asian region (27.5°N–47.5°N, 107.5°E–137.5°E) to identify the migration of precursors attributable to the SPF events at high altitudes. The model was driven by Goddard Earth Observing System-Forward Processing (GEOS-FP) assimilated meteorology data with a spatial resolution of $0.25^\circ \times 0.3125^\circ$ produced by the NASA Global Modeling and Assimilation Office (GMAO; https://gmao.gsfc.nasa.gov/GMAO_products/). For the anthropogenic emissions, the KORUS-AQ v5 emission inventory was applied, which is based on the Comprehensive Regional Emissions for Atmospheric Transport Experiment (CREATE) inventory developed by Konkuk University (Woo et al., 2012).

3. Results and discussion

3.1. Vertical distribution of aerosol number concentration during the KORUS-AQ campaign

To elaborate on the overall SPF characteristics during the KORUS-AQ campaign, the vertical profile of the number concentration of ultrafine particles with diameters between 3 nm and 10 nm ($N_{\text{CN3-10}}$) was examined. $N_{\text{CN3-10}}$ generally decreased with increasing altitudes, showing a peak of around $7606 \pm 12,003 \text{ cm}^{-3}$ below 1 km altitude (Fig. 1a), suggesting SPFs around the Korean Peninsula were primarily regarded to occur in the BL rather than the FT. Previous studies reported that NPF frequency in the BL was highest during the springtime in the polluted urban area (Park et al., 2015) as well as relatively clean regional background sites (Kim et al., 2013). Furthermore, NPF occurrence rate during the KORUS-AQ campaign (~63%) was higher than the springtime seasonal mean (Lee et al., 2021), contributing to the BL peak of $N_{\text{CN3-10}}$ in this study. Although the SPF event was observed in the FT over the polluted areas such as urban Beijing and Yangtze River Delta region (Quan et al., 2017; Qi et al., 2019), the averaged vertical profile of $N_{\text{CN3-10}}$ over Korean Peninsula was more consistent to the results from the literatures that reported the active SPF in the BL (Väänänen et al., 2016; Altstädter et al., 2018).

$N_{\text{CN3-10}}$ was generally above 6000 cm^{-3} up to the daytime BL height (~1 km) and rapidly decreased to about 3000 cm^{-3} in the vicinity of 1 km altitude. $N_{\text{CN3-10}}$ decreased even more from an altitude of about 4 km, down to ~1000 cm^{-3} . The number densities of aerosols with diameters from 10 nm to 199.5 nm were maintained over ~6000 cm^{-3} from the surface to the daytime BL height (Fig. 1b). A number density of ~3000–4000 cm^{-3} of accumulation-mode particles was observed at the 1–2 km range, possibly due to the influence of long-range transport of aged particles from upwind regions (Yu et al., 2006; Cho et al., 2021). Furthermore, particles in this size range (> 50–100 nm) can be potentially activated into cloud condensation nuclei (CCN; Rose et al., 2017). This implied that the formation of low-level clouds below 2 km altitude

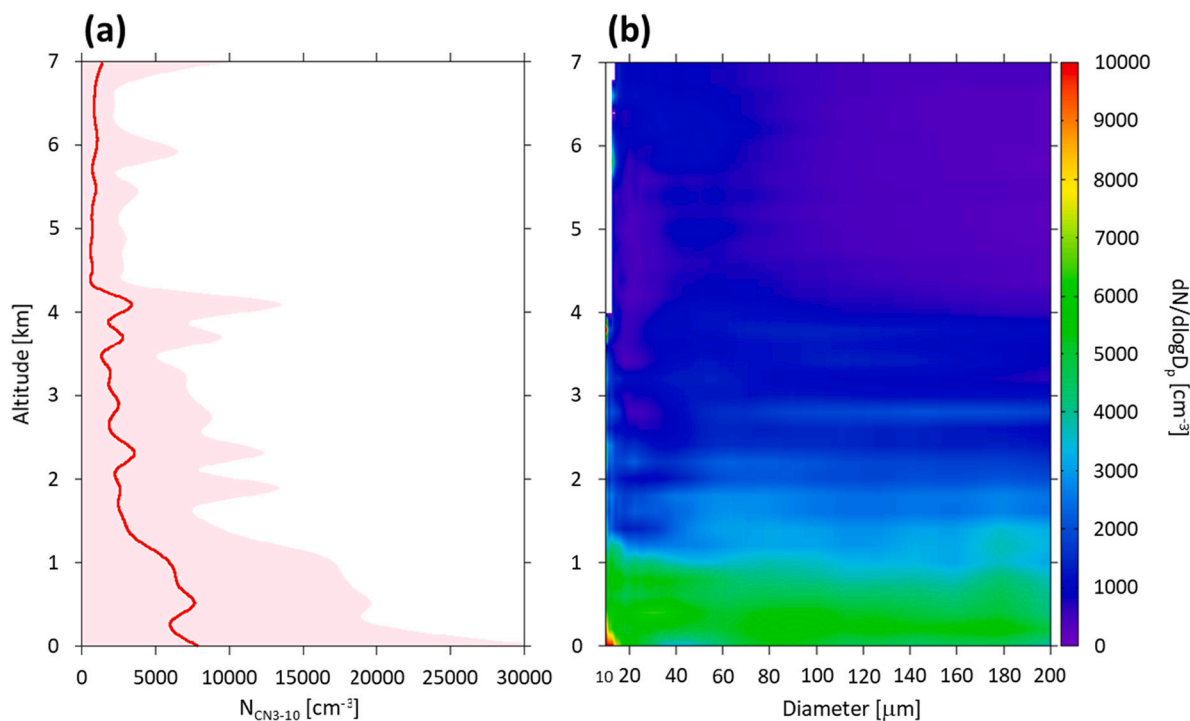


Fig. 1. (a) The vertical profile of $N_{\text{CN3-10}}$ during the KORUS-AQ campaign. The red line and pink shading denote the average and 1-standard deviation of $N_{\text{CN3-10}}$, respectively. (b) The vertical profile of number densities of aerosols with diameters from 10 nm to 199.5 nm during the KORUS-AQ campaign. (For interpretation of the references to colour in this figure legend, the reader is referred to the web version of this article.)

can be highly influenced by vertical distribution of accumulation-mode particles over Korean Peninsula under low horizontal variability of activated CCN during the KORUS-AQ campaign (Park et al., 2020). Meanwhile, the number density of nucleation-mode (~ 15 nm) particles was over $\sim 10,000$ cm^{-3} near the surface, reflecting frequent particle formation in the BL. Similar to the vertical profile of $N_{\text{CN}3-10}$ (Fig. 1a), the number densities from 10 nm to 199.5 nm (Fig. 1b) indicated almost no particles above ~ 4 km altitude.

3.2. Observations of SPF events in the boundary layer (BL) and free troposphere (FT)

SPF cases in the BL and FT during the KORUS-AQ campaign were

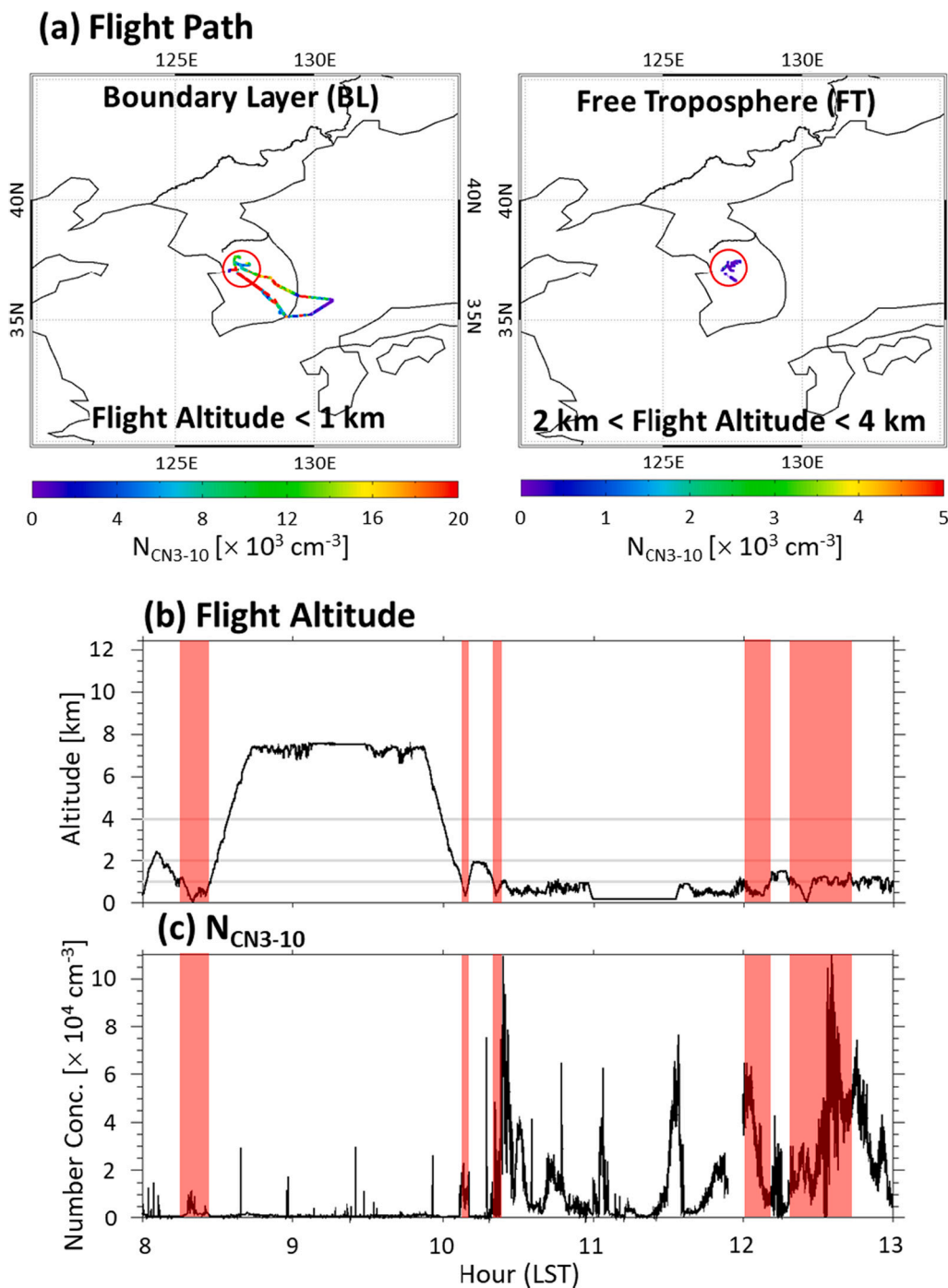


Fig. 2. BL SPF case (7 May 2016): (a) The flight path in the BL and FT. The SMA is denoted as red circle and $N_{\text{CN}3-10}$ corresponding to the flight path is represented as colour scale. (b) The time series of flight altitude. The light grey line is located at the 1 km, 2 km, 4 km altitudes and the period of BL (< 1 km) flight over SMA is shaded as red colour. (c) The time series of $N_{\text{CN}3-10}$. (For interpretation of the references to colour in this figure legend, the reader is referred to the web version of this article.)

3.2.1. BL SPF case: 7 May 2016

During 7 May, the flight route consisted of Seoul-Busan and Seoul-Pohang, and stereoscopic observations were conducted in the Seoul metropolitan area (SMA) three times (i.e., the beginning, middle, and end of the flight). In particular, the observations at altitudes from 2 to 4 km (designated as the FT in this study) were carried out only in the SMA during the day. The defined BL and FT altitudes as well as variation of flight altitude are represented in Fig. 2b. The N_{CN3-10} following the flight route was observed to be over $\sim 12,000 \text{ cm}^{-3}$ in the BL of the SMA, but negligible N_{CN3-10} was measured in the FT (Fig. 2a). Consistently, a considerable aerosol backscatter coefficient ($\sim 0.006 \text{ km}^{-1} \text{ sr}^{-1}$) was only observed below 1 km from the high spectral resolution lidar (HSRL) measurement (not shown). The N_{CN3-10} in the BL during 08:00–09:00 local standard time (LST) was as high as about $10,000 \text{ cm}^{-3}$ and increased up to $50,000\text{--}100,000 \text{ cm}^{-3}$ from 10:00 LST by the influence of SPF under the increased solar radiation (Fig. 2c; Chandra et al., 2016). Overall, 7 May was designated as a BL SPF case generated in the SMA in this study.

Fig. 3 displays the time series of major secondary inorganic species and their precursors during the BL SPF case, which are largely related to the submicron particles in East Asia. Note that the increase of secondary inorganic species cannot be only attributable to the formation of submicron particles. For example, the simultaneous increase in secondary inorganic aerosols in the morning (about 08:18 LST) can be regarded as a result influenced by the transported plume or primary emission, because the increase occurred under a relatively low N_{CN3-10} ($\sim 10,000 \text{ cm}^{-3}$) condition during 7 May. The SO_2 mixing ratio in the BL of the SMA was maintained at a range lower than about 5000 pptv during the day; however, the sulfate concentration of the BL during the day did not

show a clear increase even when the SO_2 mixing ratio increased slightly except for a few minutes after 10:00 LST. The increase of SO_2 mixing ratio was 2–3 times lower than that of NO_2 right after 10:00 LST, considering the similar scale of the variation between them during the KORUS-AQ campaign (Kim et al., 2020a). A sharp increase in the nitrate concentration can be attributable to the oxidation of NO_2 with OH or O_3 . The formation of oxidation products (HNO_3 ; nitric acid) could also be identified. Thus, the SPF over the SMA can be more attributable to the oxidation of NO_2 with OH or O_3 rather than to SO_2 -to-sulfate conversion.

Gas-phase reaction rates can positively be correlated with the temperature according to the Arrhenius equation (De Persis et al., 2004; Seinfeld and Pandis, 2016), while the aqueous-phase processes are known to occur more actively under humid environmental condition (Wu et al., 2019; Seinfeld and Pandis, 2016). Based on the theories, we can roughly look into the formation mechanisms of major secondary inorganic species during the case considered herein. It is worth mentioning that the above-mentioned period unrelated to SPF (around 8:16–8:27 LST) was excluded from the analysis. The nitrogen and sulfur oxidation ratios (NOR and SOR) were defined as the molar fraction of nitrate and sulfate: $\text{NOR} = n\text{NO}_3^- / (n\text{NO}_3^- + n\text{NO}_2)$, $\text{SOR} = n\text{SO}_4^{2-} / (n\text{SO}_4^{2-} + n\text{SO}_2)$ (Ji et al., 2018; Tian et al., 2019). The NOR during the BL SPF case was positively correlated with the air temperature ($r = 0.69$ with $p = 0.0006$; Fig. 4a) rather than RH ($r = 0.30$ with $p = 0.19$; Fig. 4b). Given that a positive correlation with air temperature can be related to the gas-phase pathways, this suggested that homogeneous gas-phase reactions of NO_2 with OH or O_3 contributed to nitrate formation over SMA. Although the primary pathways controlling the daytime nitrate formation remain controversial (Tao et al., 2018), many previous studies have reported that gas-phase pathways are predominant for

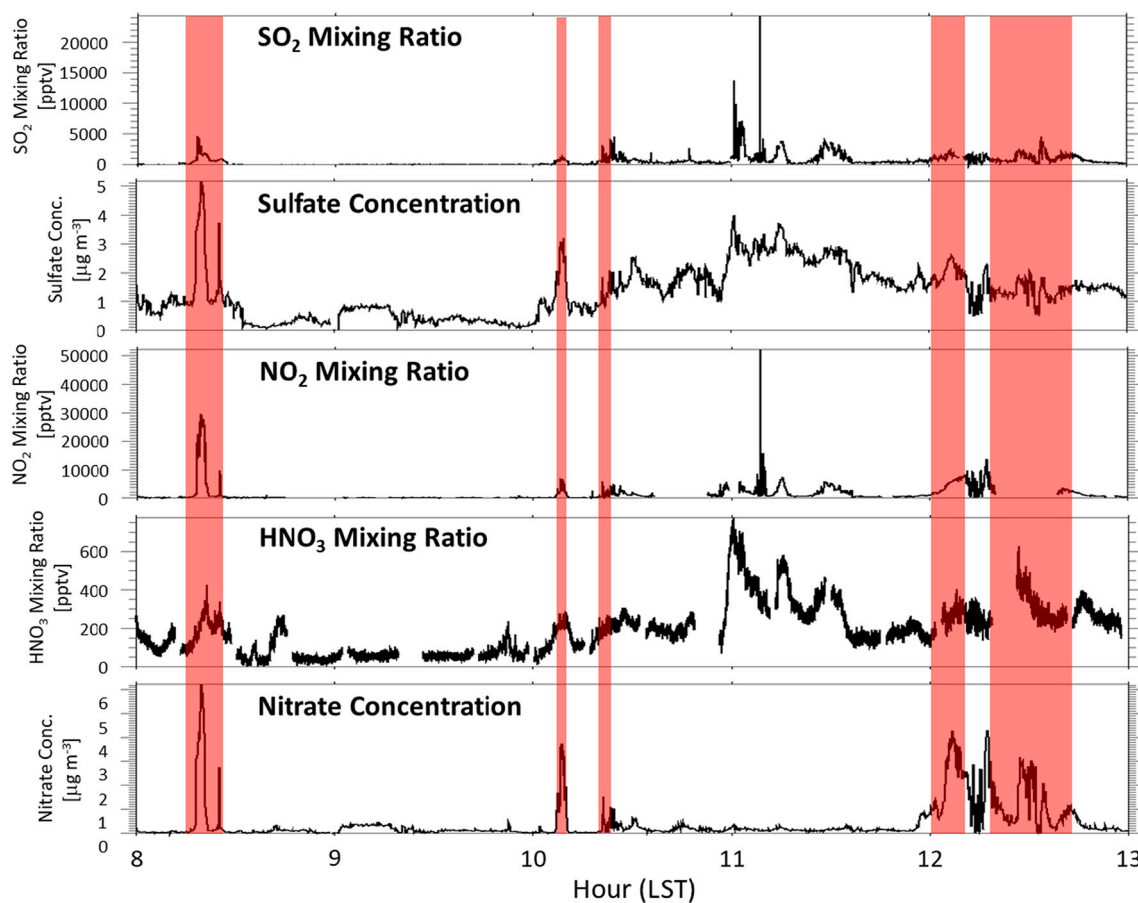


Fig. 3. The time series of SO_2 mixing ratio, sulfate concentration, NO_2 mixing ratio, HNO_3 mixing ratio, and nitrate concentration during the BL SPF case (7 May 2016). The period of BL ($< 1 \text{ km}$) flight over the SMA is shaded as red colour. (For interpretation of the references to colour in this figure legend, the reader is referred to the web version of this article.)

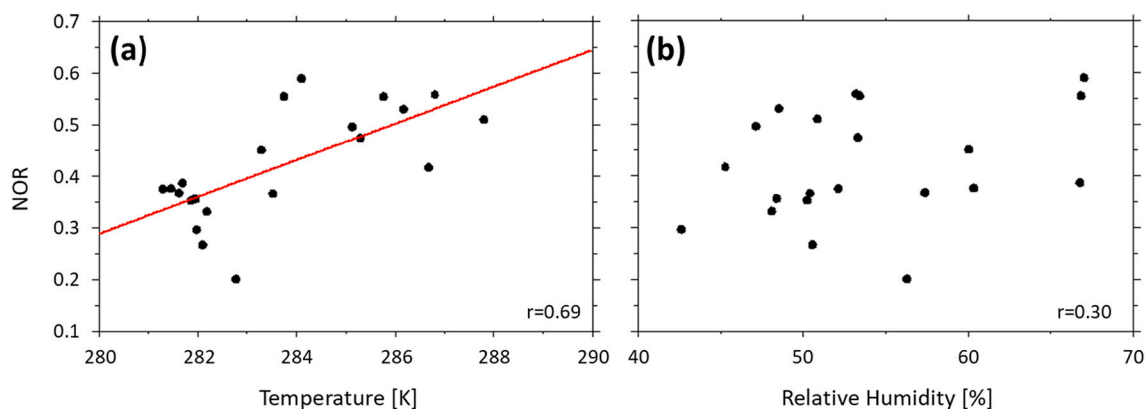


Fig. 4. The scatter plot for NOR versus (a) temperature and (b) relative humidity for DC-8 flight in BL over the SMA during the BL SPF case (7 May 2016). The linear regression line is represented as red solid line. (For interpretation of the references to colour in this figure legend, the reader is referred to the web version of this article.)

nitrate formation during the daytime (Khoder, 2002; Shen et al., 2020; Liu et al., 2020b).

By considering the abrupt increase of N_{CN3-10} as an indicator of recent SPF event (Kulmala et al., 2004; Crumeyrolle et al., 2010; Kim et al., 2014), the relationship between N_{CN3-10} ($> 10,000 \text{ cm}^{-3}$) and NOR (or SOR) measured hourly at Olympic Park in Seoul was inspected to characterize SPF in Seoul during the period of entire KORUS-AQ campaign (12 May to 10 June, Fig. 5). Because several previous studies have reported that the oxidation of SO_2 to sulfate through sulfuric acid formation could play a dominant role in the SPF in the urban boundary layer over East Asia (Zhang et al., 2004; Yue et al., 2010; Yao et al., 2018), many schemes largely deal with the formation of submicron particles as a function of the concentration of sulfuric acid (Kazil and Lovejoy, 2007; Kürten, 2019). Our analysis suggests that the absolute SOR was generally higher than NOR, indicating that the oxidation of sulfur could be more dominant than that of nitrogen during the KORUS-AQ campaign. Meanwhile, NOR had a positive correlation with N_{CN3-10} ($r = 0.45$; Fig. 5b) but SOR had little (Fig. 5a), which suggests that the relative importance of nitrogen oxidation grew compared to sulfur oxidation when the N_{CN3-10} increased. This result is consistent with previous intensive field experiments over the polluted environment (Young et al., 2016; Li et al., 2018; Chen et al., 2020). For example, Young et al. (2016) revealed that ammonium nitrate was dominant among the constituent of PM_{10} at polluted urban environment during Deriving Information on Surface Conditions from Column and Vertically Resolved Observations Relevant to Air Quality (DISCOVER-AQ) campaign.

3.2.2. FT SPF case: 31 May 2016

The 31 May case was expected to be influenced by pollutants from upwind regions (e.g., China) during the KORUS-AQ campaign (Peterson et al., 2019). To capture the impact of Chinese emissions from the observations, the DC-8 aircraft flew over the Yellow Sea (YS). The flight routes of the DC-8 during 31 May and the corresponding N_{CN3-10} values are presented in Fig. 6a. During 31 May, substantial N_{CN3-10} ($\sim 2000 \text{ cm}^{-3}$) was observed in the FT over the YS, and it even exceeded 5000 cm^{-3} in the west of the SMA. In the time series of N_{CN3-10} during 31 May (Fig. 6c), N_{CN3-10} showed peaks at around $30,000\text{--}40,000 \text{ cm}^{-3}$ during the flight in the FT, reflecting the occurrence of SPF event. About $0.006 \text{ km}^{-1} \text{ sr}^{-1}$ of backscatter coefficient was measured in the 2–3 km range under the influence of submicron particles formed in the FT (not shown). Based on these observations, 31 May was designated as the FT SPF case.

Fig. 7 displays the time series of the secondary inorganic aerosols and their precursors during the FT SPF case. Generally, the SO_2 -to-sulfate conversion seemed to highly influence the particle formation events in the FT because the sulfate concentration was changed along with the SO_2 mixing ratio. On the other hand, the NO_2 mixing ratio and nitrate concentration were nearly zero, suggesting that oxidation of NO_2 had little correlation with the SPF event on 31 May.

Because the baseline level of the SO_2 mixing ratio is typically low in the FT, a high SOR would be derived even if only a small amount of SO_2 was converted to sulfate or an abrupt variation in the SO_2 mixing ratio was induced by transport, degrading the meaning of SOR. For the FT SPF case, the sulfate-to-CO ratio was used instead of SOR because CO which has a relatively long lifetime is appropriate for tracing the change in sulfate (Ding et al., 2015). The sulfate-to-CO ratio had a positive

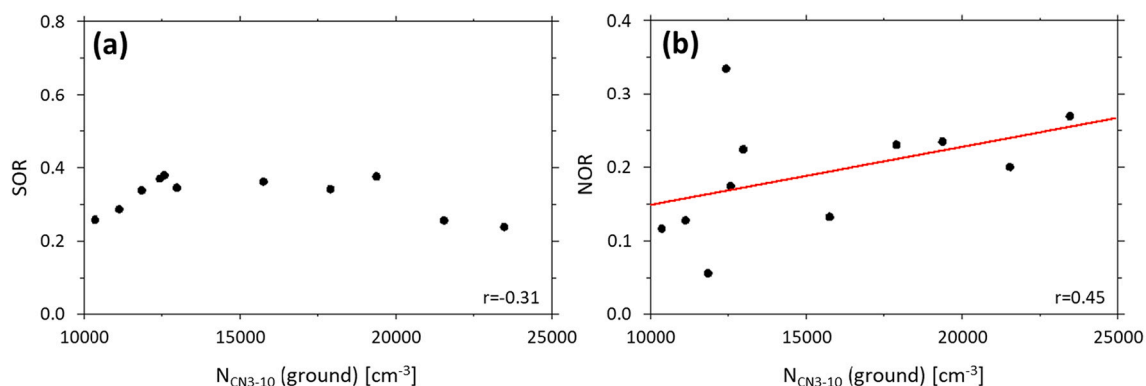


Fig. 5. The scatter plot for N_{CN3-10} ($> 10,000 \text{ cm}^{-3}$) versus (a) SOR and (b) NOR derived from the measurements at the Olympic park in Seoul for the entire KORUS-AQ period (12 May–10 June 2016). The linear regression line is represented as red solid line. (For interpretation of the references to colour in this figure legend, the reader is referred to the web version of this article.)

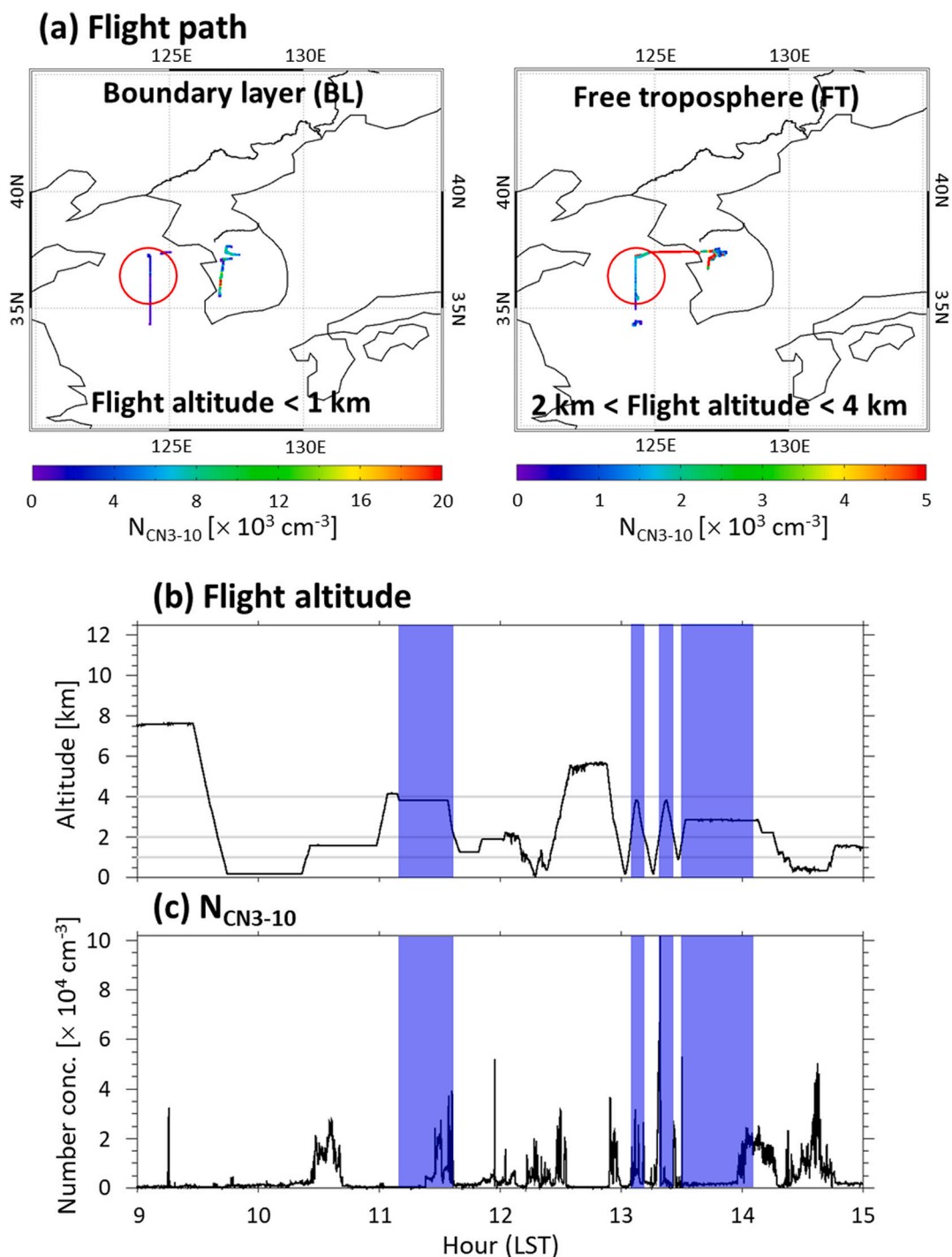


Fig. 6. Same as Fig. 2, except for the dataset for the FT SPF case (31 May 2016). The period of FT (2 km–4 km) flight over the YS is shaded as azure colour.

correlation with both the temperature and RH, indicating that aqueous-phase pathways as well as gas-phase reactions might be attributable to the sulfate formation in the FT (Fig. 8). Many studies reported that aqueous-phase oxidation of SO_2 associated with the uptake processes on the surface of preexisting particles is the main pathway of sulfate formation, although the gas-phase reactions of SO_2 are significant as well (Khoder, 2002; Tsona et al., 2018; Liu et al., 2020b); these findings are consistent with the results herein.

Due to the lack of continuous observation of atmospheric pollutants at high altitudes, the direct derivation of the general properties of SPF events in the FT during the entire KORUS-AQ campaign was limited. Rather than generalizing, investigation of the possible cause of the FT

SPF case was conducted by simulating the behavior of SO_2 at 700 hPa using a chemical transport model (GEOS-Chem; Fig. 9). The migration of SO_2 and sulfate was simulated at the 700-hPa pressure level. The mixing ratio of the transported SO_2 over the YS was expected to be maximum around 12:00 LST on 31 May, implying that the FT over the YS during 31 May could be suitable for the active sulfate formation. When the continental precursors are directly transported over the shallow marine boundary layer, the formation of particles could be facilitated in the FT under favorable conditions such as the lack of the preexisting particles and increase in the sunlight (Takegawa et al., 2020). The submicron particles produced by this mechanism can spread to FT or be entrained to the BL, thereby also having an influence on the air quality at the

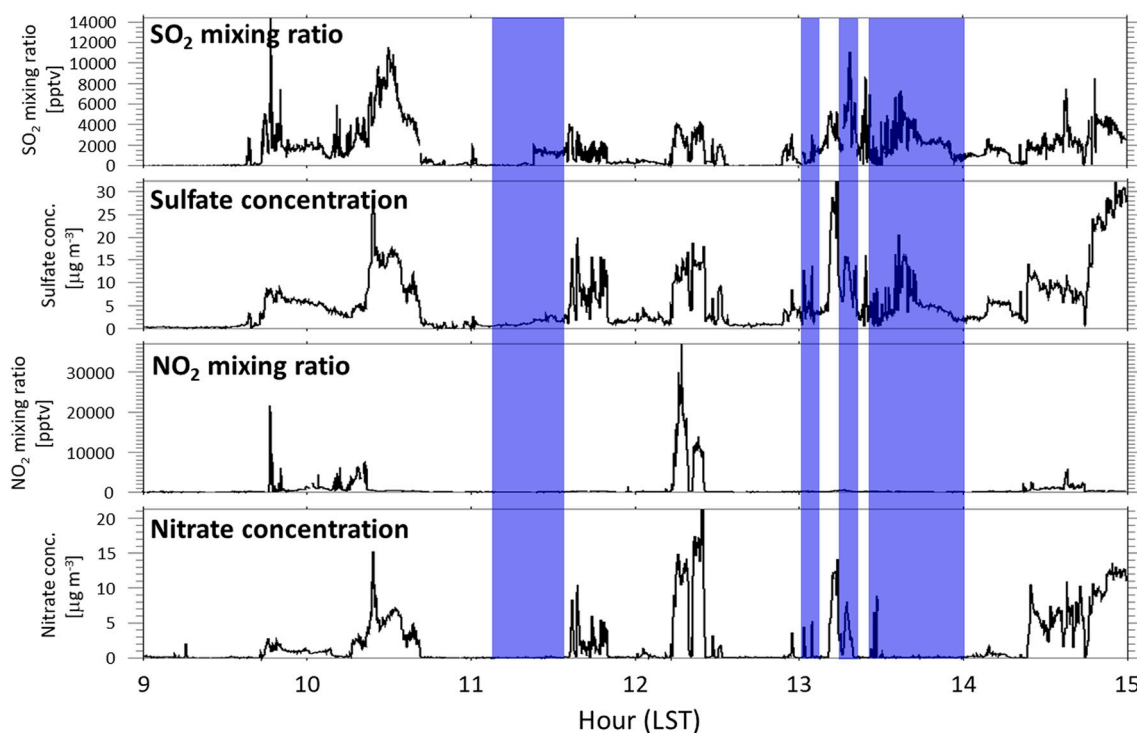


Fig. 7. Same as Fig. 3, except for the dataset for the FT SPF case (31 May 2016). The period of FT (2 km–4 km) flight over the YS is shaded as azure colour.

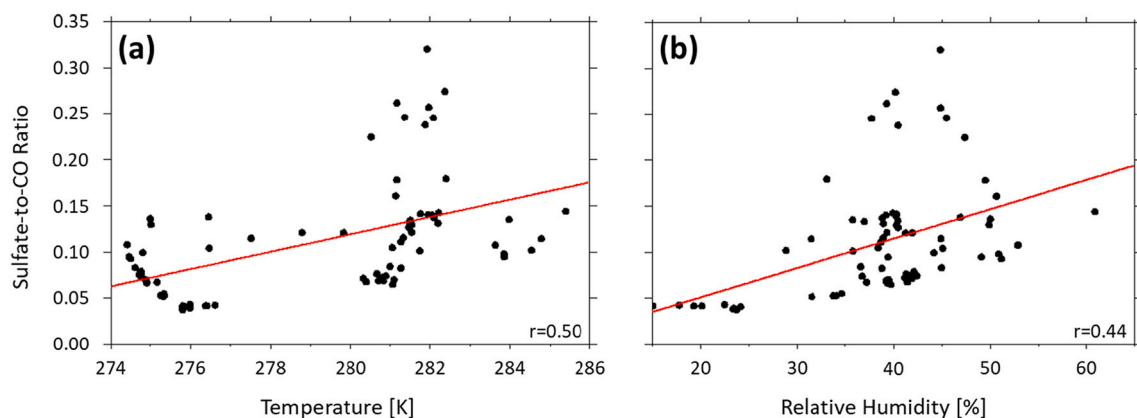


Fig. 8. The scatter plot for sulfate-to-CO ratio versus (a) temperature and (b) relative humidity for DC-8 flight in FT over the YS during the FT SPF case (31 May 2016). The linear regression lines are represented as red solid lines. (For interpretation of the references to colour in this figure legend, the reader is referred to the web version of this article.)

surface (Kerminen et al., 2018; Takegawa et al., 2020). This observation-based capture of FT SPF resulting from continental condensable vapors above shallow marine boundary layer was consistent to the formation of new particles in the FT over open seas derived from the Hydrological cycle in Mediterranean Experiment (HYMEX) project (Rose et al., 2015).

4. Summary and conclusions

We conducted a comparative analysis of the processes associated with the SPF events that occurred in the BL and the FT during the KORUS-AQ campaign (May–June 2016). Several key findings are as follows:

- N_{CN3-10} generally decreased with increasing altitudes, reaching $7606 \pm 12,003 \text{ cm}^{-3}$ in the daytime BL. In addition, the number density of particles with diameters from 10 nm to 15 nm was over $\sim 10,000 \text{ cm}^{-3}$ near the surface. Vertical distribution of nucleation-

mode particles indicated that SPF occurrence around the Korean Peninsula during the KORUS-AQ campaign was mostly observed in the BL.

- For the BL SPF event over SMA, a major secondary inorganic species responsible for the SPF event was estimated to be nitrate. A positive correlation between NOR and temperature implied that gas-phase reactions of NO_2 with OH or O_3 possibly induced nitrate formation. From the relationship between NOR (or SOR) and N_{CN3-10} ($> 10,000 \text{ cm}^{-3}$), the relative importance of nitrogen oxidation grew as the N_{CN3-10} increased.
- SO_2 -to-sulfate conversion seemed to highly influence the FT SPF event over YS. Gas-phase and aqueous-phase pathways were thought to be participated in the sulfate formation, as indicated by positive correlation of sulfate-to-CO ratio with both temperature and RH. The production of high level of SO_2 by the transport from upwind regions above the shallow marine boundary layer might be attributable to

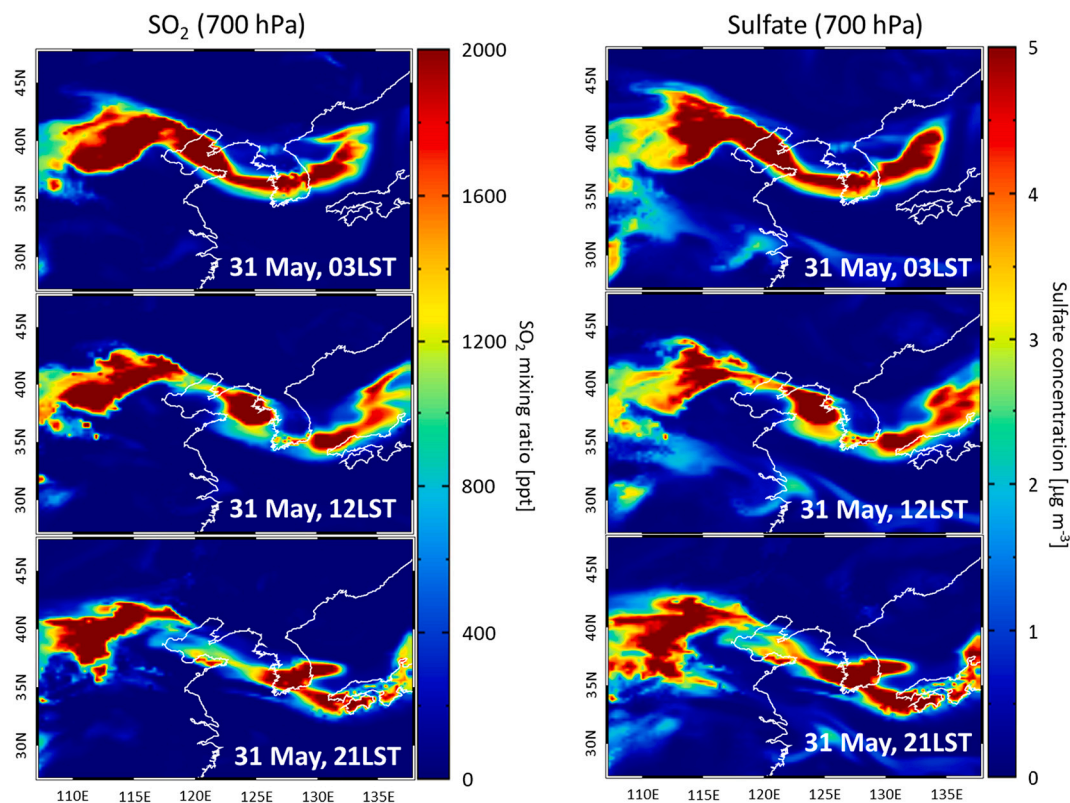


Fig. 9. The spatial distribution of SO_2 mixing ratio (left panel) and sulfate concentration (right panel) at 700 hPa simulated by GEOS-Chem for FT SPF case (31 May 2016).

the sulfate formation under the favorable conditions for the SPF in the FT.

Through the understanding of the SPF in the FT as well as BL inferred from the observations in this study, the calculation of formation rate in current schemes of the atmospheric models can be improved by taking these observed formation processes into account. Because SPF can be an effective pathway for CCN production (Rose et al., 2017; Gordon et al., 2017), radiative processes associated with the cloud properties would be understood better based on the improved schemes in future studies.

Declaration of Competing Interest

None.

Acknowledgments

The authors are grateful to the NASA DC-8 pilots and crew, and to all members of the KORUS-AQ science team for their contributions during the field campaign and the agencies operating the surface networks. This work was supported by the National Research Foundation of Korea (NRF) grant funded by the Korea government (MSIT)(No. NRF-2021R1A4A5032320).

References

- Alexander, B., Hastings, M., Allman, D., Dachs, J., Thornton, J., Kunasek, S., 2009. Quantifying atmospheric nitrate formation pathways based on a global model of the oxygen isotopic composition ($\Delta 17\text{O}$) of atmospheric nitrate. *Atmos. Chem. Phys.* 9 (14), 5043–5056. <https://doi.org/10.5194/acp-9-5043-2009>.
- Altstädter, B., Platis, A., Jähn, M., Baars, H., Lücknerath, J., Held, A., Lampert, A., Bange, J., Hermann, M., Wehner, B., 2018. Airborne observations of newly formed boundary layer aerosol particles under cloudy conditions. *Atmos. Chem. Phys.* 18 (11), 8249–8264. <https://doi.org/10.5194/acp-18-8249-2018>.
- Bey, I., Jacob, D.J., Yantosca, R.M., Logan, J.A., Field, B.D., Fiore, A.M., Li, Q., Liu, H.Y., Mickley, L.J., Schultz, M.G., 2001. Global modeling of tropospheric chemistry with

- assimilated meteorology: Model description and evaluation. *J. Geophys. Res.-Atmos.* 106 (D19), 23073–23095. <https://doi.org/10.1029/2001JD000807>.
- Bianchi, F., Tröstl, J., Junninen, H., Frege, C., Henne, S., Hoyle, C.R., Molteni, U., Herrmann, E., Adamov, A., Bukowiecki, N., Chen, X., Duplissy, J., Gysel, M., Hutterli, M., Kangasluoma, J., Kontkanen, J., Kürten, A., Manninen, H.E., Münch, S., Peräkylä, O., Petäjä, T., Rondo, L., Williamson, C., Weingartner, E., Curtius, J., Worsnop, D.R., Kulmala, M., Dommen, J., Baltensperger, U., 2016. New particle formation in the free troposphere: a question of chemistry and timing. *Science* 352 (6289), 1109–1112. <https://doi.org/10.1126/science.aad5456>.
- Chandra, I., Kim, S., Seto, T., Otani, Y., Takami, A., Yoshino, A., Irei, S., Park, K., Takamura, T., Kaneyasu, N., Hatakeyama, S., 2016. New particle formation under the influence of the long-range transport of air pollutants in East Asia. *Atmos. Environ.* 141, 30–40. <https://doi.org/10.1016/j.atmosenv.2016.06.040>.
- Chen, X., Wang, H., Lu, K., Li, C., Zhai, T., Tan, Z., Ma, X., Yang, X., Liu, Y., Chen, S., Dong, H., Li, X., Wu, Z., Hu, M., Zeng, L., Zhang, Y., 2020. Field determination of nitrate formation pathway in winter Beijing. *Environ. Sci. Technol.* 54 (15), 9243–9253. <https://doi.org/10.1021/acs.est.0c00972>.
- Cheng, Y., Zheng, G., Wei, C., Mu, Q., Zheng, B., Wang, Z., Gao, M., Zhang, Q., He, K., Carmichael, G., Pöschl, U., Su, H., 2016. Reactive nitrogen chemistry in aerosol water as a source of sulfate during haze events in China. *Sci. Adv.* 2 (12), e1601530. <https://doi.org/10.1126/sciadv.1601530>.
- Cho, C., Schwarz, J.P., Perring, A.E., Lamb, K.D., Kondo, Y., Park, J.U., Park, D.-H., Shim, K., Park, J.-S., Park, R.J., Lee, M., Song, C.-K., Kim, S.W., 2021. Light-absorption enhancement of black carbon in the Asian outflow inferred from airborne SP2 and in-situ measurements during KORUS-AQ. *Sci. Total Environ.* 773, 145531. <https://doi.org/10.1016/j.scitotenv.2021.145531>.
- Choi, J., Choi, Y., Ahn, J., Park, J., Oh, J., Lee, G., Park, T., Park, G., Owen, J.S., Lee, T., 2017. Observation of secondary organic aerosol and new particle formation at a remote site in baengnyeong Island, Korea. *Asian J. Atmos. Environ.* 11 (4), 300–312. <https://doi.org/10.5572/ajae.2017.11.4.300>.
- Choi, J., Park, R.J., Lee, H.-M., Lee, S., Jo, D.S., Jeong, J.I., Henze, D.K., Woo, J.-H., Ban, S.-J., Lee, M.-D., Lim, C.-S., Park, M.-K., Shin, H.J., Cho, S., Peterson, D., Song, C.-K., 2019. Impacts of local vs. trans-boundary emissions from different sectors on PM_{2.5} exposure in South Korea during the KORUS-AQ campaign. *Atmos. Environ.* 203, 196–205. <https://doi.org/10.1016/j.atmosenv.2019.02.008>.
- Chu, B., Dada, L., Liu, Y., Yao, L., Wang, Y., Du, W., Cai, J., Dällenbach, K., Chen, X., Simonen, P., Zhou, Y., Deng, C., Fu, Y., Yin, R., Li, H., He, X.-C., Feng, Z., Yan, C., Kangasluoma, J., Bianchi, F., Jiang, J., Kujansuu, J., Kerminen, V.-M., Petäjä, T., He, H., Kulmala, M., 2020. Particle growth with photochemical age from new particle formation to haze in the winter of Beijing, China. *Sci. Total Environ.* 753, 142207. <https://doi.org/10.1016/j.scitotenv.2020.142207>.
- Crouse, J.D., McKinney, K.A., Kwan, A.J., Wennberg, P.O., 2006. Measurement of gas-phase hydroperoxides by chemical ionization mass spectrometry. *Anal. Chem.* 78 (19), 6726–6732. <https://doi.org/10.1021/ac0604235>.

- Crumeyrolle, S., Manninen, H., Sellegrì, K., Roberts, G., Gomes, L., Kulmala, M., Weigel, R., Laj, P., Schwarzenboeck, A., 2010. New particle formation events measured on board the ATR-42 aircraft during the EUCAARI campaign. *Atmos. Chem. Phys.* 10, 6721–6735. <https://doi.org/10.5194/acp-10-6721-2010>.
- De Persis, S., Dollet, A., Teyssandier, F., 2004. Pressure dependence of gas-phase reaction rates. *J. Chem. Educ.* 81 (6), 832. <https://doi.org/10.1021/ed081p832>.
- DeCarlo, P.F., Kimmel, J.R., Trimborn, A., Northway, M.J., Jayne, J.T., Aiken, A.C., Gonin, M., Fuhrer, K., Horvath, T., Docherty, K.S., Worsnop, D.R., Jimenez, J.L., 2006. Field-deployable, high-resolution, time-of-flight aerosol mass spectrometer. *Anal. Chem.* 78 (24), 8281–8289. <https://doi.org/10.1021/ac061249n>.
- Ding, K., Liu, J., Ding, A., Liu, Q., Zhao, T., Shi, J., Han, Y., Wang, H., Jiang, F., 2015. Uplifting of carbon monoxide from biomass burning and anthropogenic sources to the free troposphere in East Asia. *Atmos. Chem. Phys.* 15, 2843–2866. <https://doi.org/10.5194/acp-15-2843-2015>.
- Gordon, H., Kirkby, J., Baltensperger, U., Bianchi, F., Breitenlechner, M., Curtius, J., Dias, A., Dommen, J., Donahue, N.M., Dunne, E.M., Duplissy, J., Ehrhart, S., Flagan, R.C., Frege, C., Fuchs, C., Hansel, A., Hoyle, C.R., Kulmala, M., Kürten, A., Lehtipalo, K., Makhmutov, V., Molteni, U., Rissanen, M.P., Stozhkov, Y., Tröstl, J., Tsagkogeorgas, G., Wagner, R., Williamson, C., Wimmer, D., Winkler, P.M., Yan, C., Carslaw, K.S., 2017. Causes and importance of new particle formation in the present-day and preindustrial atmospheres. *J. Geophys. Res. Atmospheres* 122 (16), 8739–8760. <https://doi.org/10.1002/2017JD026844>.
- Hanafi, N.H., Hassim, M.H., Noor, Z.Z., Ten, J.Y., Aris, N.M., Jalil, A., 2019. Economic Losses due to Health Hazards Caused by Haze Event in Johor Bahru, Malaysia. *E3S Web Conf.* 90, p. 01009. <https://doi.org/10.1051/e3sconf/20199001009>.
- He, H., Wang, Y., Ma, Q., Ma, J., Chu, B., Ji, D., Tang, G., Liu, C., Zhang, H., Hao, J., 2014. Mineral dust and NO_x promote the conversion of SO₂ to sulfate in heavy pollution days. *Sci. Rep.* 4, 4172. <https://doi.org/10.1038/srep04172>.
- Huey, L.G., Tanner, D., Slusher, D., Dibb, J.E., Arimoto, R., Chen, G., Davis, D., Buhr, M., Nowak, J., Mauldin III, R., Eisele, F.L., Kosciuch, E., 2004. CIMS measurements of HNO₃ and SO₂ at the South Pole during ISCAT 2000. *Atmos. Environ.* 38 (32), 5411–5421. <https://doi.org/10.1016/j.atmosenv.2004.04.037>.
- Hung, H.-M., Hoffmann, M.R., 2015. Oxidation of gas-phase SO₂ on the surfaces of acidic microdroplets: Implications for sulfate and sulfate radical anion formation in the atmospheric liquid phase. *Environ. Sci. Technol.* 49 (23), 13768–13776. <https://doi.org/10.1021/acs.est.5b01658>.
- Jeong, C.-H., Evans, G.J., 2009. Inter-comparison of a fast mobility particle sizer and a scanning mobility particle sizer incorporating an ultrafine water-based condensation particle counter. *Aerosol Sci. Technol.* 43 (4), 364–373. <https://doi.org/10.1080/02786820802662939>.
- Ji, Y., Qin, X., Wang, B., Xu, J., Shen, J., Chen, J., Huang, K., Deng, C., Yan, R., Xu, K., Zhang, T., 2018. Counteractive effects of regional transport and emission control on the formation of fine particles: a case study during the Hangzhou G20 summit. *Atmos. Chem. Phys.* 18 (18), 13581–13600. <https://doi.org/10.5194/acp-18-13581-2018>.
- Jiang, H., Lei, X., Xiao, H., Chen, D., Zeng, P., Yang, X., Wang, Z., Cheng, H., 2020. Pollution Characteristics, Chemical Compositions, and Population Health risks during the 2018 Winter Haze Episode in Jiangnan Plain, Central China. *Atmosphere* 11 (9), 954. <https://doi.org/10.3390/atmos11090954>.
- Jordan, C.E., Crawford, J.H., Beyersdorf, A.J., Eck, T.F., Halliday, H.S., Nault, B.A., Chang, L.-S., Park, J., Park, R., Lee, G., Kim, H., Ahn, J.-Y., Cho, S., Shin, H.J., Lee, J. H., Jung, J., Kim, D.-S., Lee, M., Lee, T., Whitehill, A., Szykman, J., Schueneman, M. K., Campuzano-Jost, P., Jimenez, J.L., DiGangi, J.P., Diskin, G.S., Diskin, G.S., Anderson, B.E., Moore, R.H., Ziemba, L.D., Fenn, M.A., Hair, J.W., Kuehn, R.E., Holz, R.E., Chen, G., Travis, K., Shook, M., Peterson, D.A., Lamb, K.D., Schwarz, J.P., 2020. Investigation of factors controlling PM_{2.5} variability across the South Korean Peninsula during KORUS-AQ. *Elem. Sci. Anth.* 8 <https://doi.org/10.1525/elementa.424>.
- Kazil, J., Lovejoy, E., 2007. A semi-analytical method for calculating rates of new sulfate aerosol formation from the gas phase. *Atmos. Chem. Phys.* 7, 3447–3459. <https://doi.org/10.5194/acp-7-3447-2007>.
- Kerminen, V.-M., Chen, X., Vakkari, V., Petäjä, T., Kulmala, M., Bianchi, F., 2018. Atmospheric new particle formation and growth: review of field observations. *Environ. Res. Lett.* 13 (10), 103003. <https://doi.org/10.1088/1748-9326/aadf3c>.
- Khoder, M., 2002. Atmospheric conversion of sulfur dioxide to particulate sulfate and nitrogen dioxide to particulate nitrate and gaseous nitric acid in an urban area. *Chemosphere* 49 (6), 675–684. [https://doi.org/10.1016/S0045-6535\(02\)00391-0](https://doi.org/10.1016/S0045-6535(02)00391-0).
- Kim, Y., Yoon, S.-C., Kim, S.-W., Kim, K.-Y., Lim, H.-C., Ryu, J., 2013. Observation of new particle formation and growth events in Asian continental outflow. *Atmos. Environ.* 64, 160–168. <https://doi.org/10.1016/j.atmosenv.2012.09.057>.
- Kim, Y., Kim, S.-W., Yoon, S.-C., 2014. Observation of new particle formation and growth under cloudy conditions at Gosan Climate Observatory, Korea. *Meteorog. Atmos. Phys.* 126, 81–90. <https://doi.org/10.1007/s00703-014-0336-2>.
- Kim, Y., Kim, S.-W., Yoon, S.-C., Park, J.-S., Lim, J.-H., Hong, J., Lim, H.-C., Ryu, J., Lee, C.-K., Heo, B.-H., 2016. Characteristics of formation and growth of atmospheric nanoparticles observed at four regional background sites in Korea. *Atmos. Res.* 168, 80–91. <https://doi.org/10.1016/j.atmosres.2015.08.020>.
- Kim, H., Zhang, Q., Heo, J., 2018. Influence of intense secondary aerosol formation and long-range transport on aerosol chemistry and properties in the Seoul Metropolitan Area during spring time: results from KORUS-AQ. *Atmos. Chem. Phys.* 18 (10), 7149–7168. <https://doi.org/10.5194/acp-18-7149-2018>.
- Kim, H., Gil, J., Lee, M., Jung, J., Whitehill, A., Szykman, J., Lee, G., Kim, D.-S., Cho, S., Ahn, J.-Y., Hong, J., Park, M.-S., 2020a. Factors controlling surface ozone in the Seoul Metropolitan Area during the KORUS-AQ campaign. *Elem. Sci. Anth.* 8, 46. <https://doi.org/10.1525/elementa.444>.
- Kim, N., Yum, S.S., Park, M., Park, J.S., Shin, H.J., Ahn, J.Y., 2020b. Hygroscopicity of urban aerosols and its link to size-resolved chemical composition during spring/summer in Seoul, Korea. *Atmos. Chem. Phys.* 20, 11245–11262. <https://doi.org/10.5194/acp-20-11245-2020>.
- Kim, S.-W., Heo, J., Park, J.-U., 2020c. Relationship between submicron particle formation and air mass history observed in the Asian continental outflow at Gosan, Korea, during 2008–2018. *Air Qual. Atmos. Health* 1–10. <https://doi.org/10.1007/s11869-020-00934-3>.
- Kulmala, M., Vehkamäki, H., Petäjä, T., Dal Maso, M., Lauri, A., Kerminen, V.-M., Birmili, W., McMurry, P., 2004. Formation and growth rates of ultrafine atmospheric particles: a review of observations. *J. Aerosol Sci.* 35 (2), 143–176. <https://doi.org/10.1016/j.jaerosci.2003.10.003>.
- Kürten, A., 2019. New particle formation from sulfuric acid and ammonia: nucleation and growth model based on thermodynamics derived from CLOUD measurements for a wide range of conditions. *Atmos. Chem. Phys.* 19 (7), 5033–5050. <https://doi.org/10.5194/acp-19-5033-2019>.
- Lee, Y., Park, J., Kim, P., Ghim, Y.S., 2021. New particle formation and diurnal variations in number concentrations at a rural site downwind of Seoul, Korea. *Atmos. Pollut. Res.* 12 (3), 214–223. <https://doi.org/10.1016/j.apr.2021.01.014>.
- Li, H., Zhang, Q., Zheng, B., Chen, C., Wu, N., Guo, H., Zhang, Y., Zheng, Y., He, K., 2018. Nitrate-driven urban haze pollution during summertime over the North China Plain. *Atmos. Chem. Phys.* 18 (8), 5293–5306. <https://doi.org/10.5194/acp-18-5293-2018>.
- Liu, C., Zhang, F., Miao, L., Lei, Y., Yang, Q., 2019. Future haze events in Beijing, China: when climate warms by 1.5 and 2.0 °C. *Int. J. Climatol.* 40 (8), 3689–3700. <https://doi.org/10.1002/joc.6421>.
- Liu, L., Bei, N., Hu, B., Wu, J., Liu, S., Li, X., Wang, R., Liu, Z., Shen, Z., Li, G., 2020a. Wintertime nitrate formation pathways in the North China plain: Importance of N₂O₅ heterogeneous hydrolysis. *Environ. Pollut.* 266, 115287. <https://doi.org/10.1016/j.envpol.2020.115287>.
- Liu, P., Ye, C., Xue, C., Zhang, C., Mu, Y., Sun, X., 2020b. Formation mechanisms of atmospheric nitrate and sulfate during the winter haze pollution periods in Beijing: gas-phase, heterogeneous and aqueous-phase chemistry. *Atmos. Chem. Phys.* 20 (7), 4153–4165. <https://doi.org/10.5194/acp-20-4153-2020>.
- Lv, G., Sui, X., Chen, J., Jayaratne, R., Mellouki, A., 2018. Investigation of new particle formation at the summit of Mt. Tai, China. *Atmos. Chem. Phys.* 18 (3), 2243–2258. <https://doi.org/10.5194/acp-18-2243-2018>.
- Mylly, N., Chee, S., Olenius, T., Lawler, M., Smith, J., 2019. Molecular-level understanding of synergistic effects in sulfuric acid–amine–ammonia mixed clusters. *J. Phys. Chem. A* 123 (12), 2420–2425. <https://doi.org/10.1021/acs.jpca.9b00909>.
- National Institute of Environmental Research (NIER), National Aeronautics and Space Administration (NASA), 2017. Rapid Science Synthesis Report. <https://espo.nasa.gov/sites/default/files/documents/KORUS-AQ-RSSR.pdf> (last access: 28 December 2020).
- Nowlan, C.R., Liu, X., Leitch, J.W., Chance, K., Gonzalez Abad, G., Liu, C., Zoogman, P., Cole, J., Delker, T., Good, W., Murracay, F., Ruppert, L., Soo, D., Follette-Cook, M.B., Janz, S.J., Kowalewski, M.G., Loughner, C.P., Pickering, K.E., Herman, J.R., Beaver, M.R., Long, R.W., Szykman, J.J., Judd, L.M., Kelley, P., Luke, W.T., Ren, X., Al-Saadi, J.A., 2016. Nitrogen dioxide observations from the Geostationary Trace gas and Aerosol Sensor Optimization (GeoTASO) airborne instrument: retrieval algorithm and measurements during DISCOVER-AQ Texas 2013. *Atmos. Meas. Tech.* 9, 2647–2668. <https://doi.org/10.5194/amt-9-2647-2016>.
- Oak, Y.J., Park, R.J., Schroeder, J.R., Crawford, J.H., Blake, D.R., Weinheimer, A.J., Woo, J.-H., Kim, S.-W., Yeo, H., Fried, A., Wisthaler, A., Brune, W.H., 2019. Evaluation of simulated O₃ production efficiency during the KORUS-AQ campaign: Implications for anthropogenic NO_x emissions in Korea. *Elem. Sci. Anth.* 7, 56. <https://doi.org/10.1525/elementa.394>.
- Park, M., Yum, S.S., Kim, J.H., 2015. Characteristics of submicron aerosol number size distribution and new particle formation events measured in Seoul, Korea, during 2004–2012. *Asia-Pac. J. Atmos. Sci.* 51 (1), 1–10. <https://doi.org/10.1007/s13143-014-0055-0>.
- Park, M., Yum, S.S., Kim, N., Anderson, B.E., Beyersdorf, A., Thornhill, K.L., 2020. On the submicron aerosol distributions and CCN activity in and around the Korean Peninsula measured onboard the NASA DC-8 research aircraft during the KORUS-AQ field campaign. *Atmos. Res.* 243, 105004. <https://doi.org/10.1016/j.atmosres.2020.105004>.
- Park, D.-H., Kim, S.-W., Kim, M.-H., Yeo, H., Park, S.S., Nishizawa, T., Shimizu, A., Kim, C.-H., 2021. Impacts of local versus long-range transported aerosols on PM₁₀ concentrations in Seoul, Korea: An estimate based on 11-year PM₁₀ and lidar observations. *Sci. Total Environ.* 750, 141739. <https://doi.org/10.1016/j.scitotenv.2020.141739>.
- Peterson, D.A., Hyer, E.J., Han, S.-O., Crawford, J.H., Park, R.J., Holz, R., Kuehn, R.E., Eloranta, E., Knote, C., Jordan, C.E., Lefer, B.L., 2019. Meteorology influencing springtime air quality, pollution transport, and visibility in Korea. *Elem. Sci. Anth.* 7, 57. <https://doi.org/10.1525/elementa.395>.
- Qi, X., Ding, A., Nie, W., Chi, X., Huang, X., Xu, Z., Wang, T., Wang, Z., Wang, J., Sun, P., Zhang, Q., Huo, J., Wang, D., Bian, Q., Zhou, L., Zhang, Q., Ning, Z., Fei, D., Xiu, G., Fu, Q., 2019. Direct measurement of new particle formation based on tethered airship around the top of the planetary boundary layer in eastern China. *Atmos. Environ.* 209, 92–101. <https://doi.org/10.1016/j.atmosenv.2019.04.024>.
- Quan, J., Liu, Y., Liu, Q., Jia, X., Gao, Y., Gao, Y., Ding, D., Li, J., Wang, Z., 2017. Anthropogenic pollution elevates the peak height of new particle formation from planetary boundary layer to lower free troposphere. *Geophys. Res. Lett.* 44 (14), 7537–7543. <https://doi.org/10.1002/2017GL074553>.

- Richards, L.W., 1983. Comments on the oxidation of NO₂ to nitrate—day and night. *Atmos. Environ.* (1967) 17 (2), 397–402. [https://doi.org/10.1016/0004-6981\(83\)90057-4](https://doi.org/10.1016/0004-6981(83)90057-4).
- Rodríguez, S., González, Y., Cuevas, E., Ramos, R., Romero, P.M., Abreu-Afonso, J., Redondas, A., 2009. Atmospheric nanoparticle observations in the low free troposphere during upward orographic flows at Izaña Mountain Observatory. *Atmos. Chem. Phys.* 9 (17), 6319–6335. <https://doi.org/10.5194/acp-9-6319-2009>.
- Rose, C., Sellegrì, K., Freney, E., Dupuy, R., Colomb, A., Pichon, J.M., Ribeiro, M., Bourianne, T., Burnet, F., Schwarzenboeck, A., 2015. Airborne measurements of new particle formation in the free troposphere above the Mediterranean Sea during the HYMEX campaign. *Atmos. Chem. Phys.* 15 (17), 10203–10218. <https://doi.org/10.5194/acp-15-10203-2015>.
- Rose, C., Sellegrì, K., Moreno, I., Velarde, F., Ramonet, M., Weinhold, K., Krejci, R., Andrade, M., Wiedensohler, A., Ginot, P., Laj, P., 2017. CCN production by new particle formation in the free troposphere. *Atmos. Chem. Phys.* 17 (2), 1529–1541. <https://doi.org/10.5194/acp-17-1529-2017>.
- Russell, A.G., Cass, G.R., Seinfeld, J.H., 1986. On some aspects of nighttime atmospheric chemistry. *Environ. Sci. Technol.* 20 (11), 1167–1172. <https://pubs.acs.org/doi/pdf/10.1021/es00153a013> (last access: 28 December 2020).
- Sander, S.P., Seinfeld, J.H., 1976. Chemical kinetics of homogeneous atmospheric oxidation of sulfur dioxide. *Environ. Sci. Technol.* 10 (12), 1114–1123. <https://pubs.acs.org/doi/pdf/10.1021/es60122a007> (last access: 28 December 2020).
- Seinfeld, J.H., Pandis, S.N., 2016. *Atmospheric Chemistry and Physics*.
- Shen, X., Sun, J., Zhang, X., Kivekäs, N., Zhang, Y., Wang, T., Zhang, X., Yang, Y., Wang, D., Qin, D., 2016. Particle climatology in Central East China retrieved from measurements in planetary boundary layer and in free troposphere at a 1500-m-High mountaintop site. *Aerosol Air Qual. Res.* 16 (3), 689–701. <https://doi.org/10.4209/aaqr.2015.02.0070>.
- Shen, X., Sun, J., Kivekäs, N., Kristensson, A., Zhang, X., Zhang, Y., Zhang, L., Fan, R., Qi, X., Ma, Q., Zhou, H., 2018. Spatial distribution and occurrence probability of regional new particle formation events in eastern China. *Atmos. Chem. Phys.* 18 (2), 587–599. <https://doi.org/10.5194/acp-18-587-2018>.
- Shen, J., Zhao, Q., Cheng, Z., Wang, P., Ying, Q., Liu, J., Duan, Y., Fu, Q., 2020. Insights into source origins and formation mechanisms of nitrate during winter haze episodes in the Yangtze River Delta. *Sci. Total Environ.* 741, 140187. <https://doi.org/10.1016/j.scitotenv.2020.140187>.
- Slusher, D.L., Huey, L.G., Tanner, D.J., Flocke, F.M., Roberts, J.M., 2004. A thermal dissociation–chemical ionization mass spectrometry (TD–CIMS) technique for the simultaneous measurement of peroxyacetyl nitrates and dinitrogen pentoxide. *J. Geophys. Res.-Atmos.* 109, D19315. <https://doi.org/10.1029/2004JD004670>.
- Song, M., Lee, M., Kim, J.H., Yum, S.S., Lee, G., Kim, K.-R., 2010. New particle formation and growth in relation to vertical mixing and chemical species during ABC-EAREX2005. *Atmos. Res.* 97 (3), 359–370. <https://doi.org/10.1016/j.atmosres.2010.04.013>.
- Takegawa, N., Seto, T., Moteki, N., Koike, M., Oshima, N., Adachi, K., Kita, K., Takami, A., Kondo, Y., 2020. Enhanced new particle formation above the marine boundary layer over the Yellow Sea: potential impacts on cloud condensation nuclei. *J. Geophys. Res.-Atmos.* 125 (9), e2019JD031448. <https://doi.org/10.1029/2019JD031448>.
- Tao, J., Zhang, Z., Tan, H., Zhang, L., Wu, Y., Sun, J., Che, H., Cao, J., Cheng, P., Chen, L., Zhang, R., 2018. Observational evidence of cloud processes contributing to daytime elevated nitrate in an urban atmosphere. *Atmos. Environ.* 186, 209–215. <https://doi.org/10.1016/j.atmosenv.2018.05.040>.
- Tian, M., Liu, Y., Yang, F., Zhang, L., Peng, C., Chen, Y., Shi, G., Wang, H., Luo, B., Jiang, C., Li, B., Takeda, N., Koizumi, K., 2019. Increasing importance of nitrate formation for heavy aerosol pollution in two megacities in Sichuan Basin, Southwest China. *Environ. Pollut.* 250, 898–905. <https://doi.org/10.1016/j.envpol.2019.04.098>.
- Tsona, N.T., Li, J., Du, L., 2018. From O₂–initiated SO₂ oxidation to sulfate formation in the gas phase. *J. Phys. Chem. A* 122 (27), 5781–5788. <https://doi.org/10.1021/acs.jpca.8b03381>.
- Väänänen, R., Krejci, R., Manninen, H.E., Manninen, A., Lampilahti, J., Buenrostro Mazon, S., Nieminen, T., Yli-Juuti, T., Kontkanen, J., Asmi, A., Aalto, P., Keronen, P., Pohja, T., O'Connor, E., Kerminen, V.-M., Petäjä, T., Kulmala, M., 2016. Vertical and horizontal variation of aerosol number size distribution in the boreal environment. *Atmos. Chem. Phys. Discuss.* 1–43. <https://doi.org/10.5194/acp-2016-556>.
- Wang, G., Zhang, R., Gomez, M.E., Yang, L., Zamora, M.L., Hu, M., Lin, Y., Peng, J., Guo, S., Meng, J., Li, J., Cheng, C., Hu, T., Ren, Y., Wang, Y., Gao, J., Cao, J., An, Z., Zhou, W., Li, G., Wang, J., Tian, P., Marrero-Ortiz, W., Secrest, J., Du, Z., Zheng, J., Shang, D., Zeng, L., Shao, M., Wang, W., Huang, Y., Wang, Y., Zhu, Y., Li, Y., Hu, J., Pan, B., Cai, L., Cheng, Y., Ji, Y., Zhang, F., Rosenfeld, D., Liss, P.S., Duce, R.A., Kolb, C.E., Mario, J.M., 2016. Persistent sulfate formation from London Fog to Chinese haze. *Proc. Natl. Acad. Sci. U. S. A.* 113 (48), 13630–13635. <https://doi.org/10.1073/pnas.1616540113>.
- Weinheimer, A., Walega, J., Ridley, B., Sachse, G., Anderson, B., Collins Jr., J., 1993. Stratospheric Noy measurements on the NASA DC-8 during AASE II. *Geophys. Res. Lett.* 20 (22), 2563–2566. <https://doi.org/10.1029/93GL02627>.
- Woo, J.-H., Choi, K.-C., Kim, H.K., Baek, B.H., Jang, M., Eum, J.-H., Song, C.H., Ma, Y.-I., Sunwoo, Y., Chang, L.-S., Yoo, S.H., 2012. Development of an anthropogenic emissions processing system for Asia using SMOKE. *Atmos. Environ.* 58, 5–13. <https://doi.org/10.1016/j.atmosenv.2011.10.042>.
- Wu, L., Sun, J., Zhang, X., Zhang, Y., Wang, Y., Zhong, J., Yang, Y., 2019. Aqueous-phase reactions occurred in the PM_{2.5} cumulative explosive growth during the heavy pollution episode (HPE) in 2016 Beijing wintertime. *Tellus Ser. B Chem. Phys. Meteorol.* 71 (1), 1620079. <https://doi.org/10.1080/16000889.2019.1620079>.
- Yao, L., Garmash, O., Bianchi, F., Zheng, J., Yan, C., Kontkanen, J., Junninen, H., Mazon, S.B., Ehn, M., Paasonen, P., Sipilä, M., Wang, M., Wang, X., Xiao, S., Chen, H., Lu, Y., Zhang, B., Wang, D., Fu, Q., Geng, F., Li, L., Wang, H., Qiao, L., Yang, X., Chen, J., Kerminen, V.-M., Petäjä, T., Worsnop, D.R., Kulmala, M., Wang, L., 2018. Atmospheric new particle formation from sulfuric acid and amines in a Chinese megacity. *Science* 361 (6399), 278–281. <https://doi.org/10.1126/science.aao4839>.
- Young, D.E., Kim, H., Parworth, C., Zhou, S., Zhang, X., Cappa, C.D., Seco, R., Kim, S., Zhang, Q., 2016. Influences of emission sources and meteorology on aerosol chemistry in a polluted urban environment: results from DISCOVER-AQ California. *Atmos. Chem. Phys.* 16 (8), 5427–5451. <https://doi.org/10.5194/acp-16-5427-2016>.
- Yu, X., Cheng, T., Chen, J., Liu, Y., 2006. A comparison of dust properties between China continent and Korea, Japan in East Asia. *Atmos. Environ.* 40 (30), 5787–5797. <https://doi.org/10.1016/j.atmosenv.2006.05.013>.
- Yue, D., Hu, M., Zhang, R., Wang, Z., Zheng, J., Wu, Z., Wiedensohler, A., He, L., Huang, X., Zhu, T., 2010. The roles of sulfuric acid in new particle formation and growth in the mega-city of Beijing. *Atmos. Chem. Phys.* 10, 4953–4960. <https://doi.org/10.5194/acp-10-4953-2010>.
- Zeng, W., Liu, T., Du, Q., Li, J., Xiao, J., Guo, L., Li, X., Xu, Y., Xu, X., Wan, D., Ma, W., 2020. The interplay of haze characteristics on mortality in the Pearl River Delta of China. *Environ. Res.* 184, 109279. <https://doi.org/10.1016/j.envres.2020.109279>.
- Zhang, Q., Stanier, C.O., Canagaratna, M.R., Jayne, J.T., Worsnop, D.R., Pandis, S.N., Jimenez, J.L., 2004. Insights into the chemistry of new particle formation and growth events in Pittsburgh based on aerosol mass spectrometry. *Environ. Sci. Technol.* 38 (18), 4797–4809. <https://doi.org/10.1021/es035417u>.